

The Dependence of Quasar Variability on Black Hole Mass

M. Wold^{1*}, M. S. Brotherton^{2†}, and Zhaohui Shang^{2‡}

¹*European Southern Observatory, Karl-Schwarzschildstr. 2, 85748 Garching bei München, Germany*

²*Department of Physics and Astronomy, University of Wyoming, Laramie, WY, 82072, U.S.A.*

16 July 2018

ABSTRACT

In order to investigate the dependence of quasar variability on fundamental physical parameters like black hole mass, we have matched quasars from the QUEST1 Variability Survey with broad-lined objects from the Sloan Digital Sky Survey. The matched sample contains ≈ 100 quasars, and the Sloan spectra are used to estimate black hole masses and bolometric luminosities. Variability amplitudes are measured from the QUEST1 light curves. We find that black hole mass correlates with several measures of the variability amplitude at the 99% significance level or better. The correlation does not appear to be caused by obvious selection effects inherent to flux-limited quasar samples, host galaxy contamination or other well-known correlations between quasar variability and luminosity/redshift. We evaluate variability as a function of rest-frame time lag using structure functions, and find further support for the variability–black hole mass correlation. The correlation is strongest for time lags of the order a few months up to the QUEST1 maximum temporal resolution of ≈ 2 years, and may provide important clues for understanding the long-standing problem of the origin of quasar optical variability. We discuss whether our result is a manifestation of a relation between characteristic variability timescale and black hole mass, where the variability timescale is typical for accretion disk thermal timescales, but find little support for this. Our favoured explanation is that more massive black holes have larger variability amplitudes, and we highlight the need for larger samples with more complete temporal sampling to test the robustness of this result.

Key words: quasars: general

1 INTRODUCTION

Quasars have been recognized as optically variable since their discovery, varying on timescales from hours to decades. The optical variability is, at best, characterized as poorly understood, but is nevertheless recognized as a means of probing physical scales that cannot be resolved spatially by any telescope or instrument (e.g. Blandford & McKee 1982; Netzer & Peterson 1997; Peterson et al. 2004). Variability is therefore an important diagnostic of the physical processes responsible for the activity of active galactic nuclei (AGN).

Quasar light curves do not show evidence for periodicities, eclipses, or any other easily understood signature. However, optical-UV quasar variability has been studied for quite some time, and observational trends between variability and other quasar properties such as luminos-

ity and redshift are comfortably established, and selection effects reasonably well understood (Giallongo, Trevese & Vagnetti 1996; Cristiani et al. 1996; Cid Fernandes, Aretxaga & Terlevich 1996; Ulrich, Maraschi & Urry 1997). For instance, variability is found to be inversely correlated with the optical luminosity of the quasar, and it has been demonstrated that, in their brighter phases of variability, quasars become bluer (e.g. Angione & Smith 1972; Hook et al. 1994; Cid Fernandes et al. 1996; Giveon et al. 1999; Webb & Malkan 2000; Vanden Berk et al. 2004). Such a bluening, or hardening, of quasar spectra during their brighter phases is likely due to the fact that two different spectral components with different variability properties make up the continuum (e.g. Ulrich et al. 1997). Quasars are also found to be increasingly variable at longer timescales, at least up to timescales of years (Hook et al. 1994; Cristiani et al. 1996; Collier & Peterson 2001). Finally, a correlation between variability and redshift is also observed, with quasars being more variable at higher redshifts (e.g. Cristiani et al. 1990; Hook et al. 1994). This cor-

* E-mail: mwold@eso.org

† E-mail: mbrother@uwyo.edu (MSB), ESO Visitor

‡ E-mail: shang@uwyo.edu

relation is apparently understood as a selection effect arising because of the chromatic nature of the variability. As quasars are more variable in the blue, and because shorter rest-frame wavelengths are probed at higher redshifts, the net effect is a correlation between redshift and variability (Giallongo et al. 1991; Cristiani et al. 1996; Cid Fernandes et al. 1996).

Radio-selected quasars do not show the anti-correlation between variability and optical luminosity, but are seen to be bluer in the brighter phases of their variability, just as optically selected quasars. (Helfand et al. 2001; Enya et al. 2002; Vanden Berk et al. 2004). Helfand et al. find that radio-selected quasars also do not show a correlation between variability and radio luminosity, but that the most radio-loud quasars may be marginally more variable than the radio-quiet (see also Enya et al. 2002; Vanden Berk et al. 2004; Rengstorf et al. 2006). Some radio-loud quasars, the blazars, are extremely variable on short timescales and likely have relativistically beamed jets pointed close to the line of sight. This kind of variability is understood at some level, and is less mysterious than the more general fluctuations seen in unbeamed quasar continua.

Vanden Berk et al. (2004), analyzing by far the largest sample of quasars ($> 25,000$ from the Sloan Digital Sky Survey or SDSS) claim that there is evidence for redshift evolution in quasar variability with quasars becoming more variable at higher redshifts. They suggest that this may reflect changes in the quasar population or in the mechanism causing the variability. Note that this effect is evolutionary and different from the variability–redshift correlation observed in other samples and explained as a selection effect (Giallongo et al. 1991; Cristiani et al. 1996; Cid Fernandes et al. 1996; Trèvese & Vagnetti 2002).

A number of models have been proposed to explain optical-UV quasar variability and the observed trends with quasar properties. At the most fundamental level, and clearly most important on the longest timescales, is the accretion rate. It is less clear if accretion rate variations, and perhaps corresponding disk temperature changes, are at the heart of variations on the timescales of years, although such changes can also account for the color changes (e.g. Pereyra et al. 2006). Disk instabilities have also been invoked (Kawaguchi et al. 1998). Others have proposed that stellar processes contribute, such as stellar collisions (Torricelli-Ciamponi et al. 2000) or supernovae (Terlevich et al. 1992; Aretxaga & Terlevich 1994; Aretxaga, Cid Fernandes & Terlevich 1997; Cid Fernandes, Aretxaga & Vieira da Silva 2000). Microlensing is an important source of variability in some lensed quasars (e.g. Refsdal et al. 2000; Morgan et al. 2006), and may more generally be important. Processes intrinsic to the central engine itself must dominate, at least above some luminosity level, since photoionized emission lines are seen to respond to continuum changes after some delay.

It has been difficult to distinguish between the different models from existing observational data. The majority of the proposed models have all been shown to be qualitatively in agreement with observations. One way of attempting to narrow down the number of possible models, and also to help constraining existing models, is to find relationships between variability and other AGN parameters, such as black hole mass. The black hole mass is a fundamental parameter of the AGN, and the discovery of such a relationship – or

lack thereof – may provide additional clues to the physical mechanisms behind the variability.

Quasar variability has already led to the measurement of black hole masses. Reverberation mapping uses spectrophotometric monitoring to determine the time lag between continuum variation and the response from broad emission lines like $H\beta$. Due to the finite speed of light, this time lag corresponds to a size scale of the line-emitting region. In combination with the velocity dispersion of the gas in the variable line-emitting region, the size scale can be used to infer a virial mass for the central black hole (e.g. Peterson et al. 2004). The time lags, and sizes, correlate with quasar luminosity (e.g. Kaspi et al. 2000, 2005), and the instantaneous velocity dispersion may therefore be used as a stand-in for the variable component of the line width, thus permitting single-epoch observations of quasars to be used for estimating black hole masses (Vestergaard 2002; Vestergaard & Peterson 2006).

The capability of making single-epoch estimates of black hole masses, even with uncertainties of factors of several, is powerful since AGN black hole masses span orders of magnitudes, from millions to billions of solar masses, and tens of thousands of spectra are available from recent surveys. Less readily available are good quality light curves of very many quasars, although surveys taking advantage of new technologies are making up for this. We have utilized these new surveys to search for relationships between quasar variability and fundamental AGN parameters, like black hole mass.

In the next section we describe how we defined a sample of quasars by matching sources from the QUEST1¹ Variability Survey (Rengstorf et al. 2004b) and the SDSS data release 2 (DR2) (Abazajian et al. 2004). We explain how data from the two surveys were used to obtain measurements of variability and black hole mass. The analysis is carried out as described in Section 3 using correlation statistics and structure functions. A number of selection effects are investigated as possible causes for the observed correlation between black hole mass and variability amplitude, and we discuss the results in Section 4. The conclusions are drawn in Section 5.

Throughout we have assumed a cosmology with $H_0 = 70 \text{ km s}^{-1} \text{ Mpc}^{-1}$, $\Omega_m = 0.3$ and $\Omega_\Lambda = 0.7$.

2 SAMPLE, DATA, AND MEASUREMENTS

Table 1 lists the 104 quasars in our sample, along with black hole masses, bolometric luminosities, Eddington ratios, and assorted variability parameters. The following sections provide details.

2.1 Sample

The sample was formed by matching objects categorized as having broad emission lines at redshifts $z < 0.75$ in the SDSS DR2 (Abazajian et al. 2004) with sources in the 200k Light Curve Catalogue of the QUEST1 Variability Survey (Rengstorf et al. 2004b). The redshift constraint was chosen for two reasons. Firstly, to ensure that the $H\beta$ would lie

¹ QUasar Equatorial Survey Team, Phase 1

within the SDSS spectral coverage hence permitting consistent black hole mass estimates using well established techniques, and, secondly, to limit the extent of time dilation effects which might introduce biases.

We find 108 matches meeting our selection criteria, with 86 sources recovered in the SDSS QSO catalogue (Schneider et al. 2005, based on DR3). The 22 sources that were not recovered in the QSO catalogue are among the less luminous and probably did not satisfy the absolute magnitude criterion of the SDSS QSO catalogue. We include the 22 sources, which all have typical quasar spectra, in our sample. Four sources were rejected on the basis of poor spectral quality, hence our final sample consists of 104 quasars.

2.2 Black Hole Mass Estimation

We estimate virial black hole masses for the quasars based on single-epoch SDSS spectra and the scaling relationships and formalism of Vestergaard & Peterson (2006). In order to do this, a measurement of the velocity dispersion of the $H\beta$ line and the continuum luminosity are required.

We begin with the SDSS spectra, which were dereddened using the Galactic extinction values of Schlegel, Finkbeiner & Davis (1998). Thereafter, the $H\beta$ region of each spectrum was fitted using the same techniques as Shang et al. (2005). The spectra are fitted from 4250 to 6000 Å using the IRAF task *specfit* (Kriss 1994) and the region is modeled with the following components: a power-law continuum, a broadened optical FeII template (Boroson & Green 1992), a host galaxy contribution based on stellar synthesis population models (Bruzual & Charlot 2003), and the $H\gamma$, $H\beta$, and $\text{O3 } \lambda\lambda 4959, 5007$ emission lines. The $H\beta$ line is fit with two broader Gaussians, plus a very narrow Gaussian constrained to match the width of the O3 line to account for the occasionally strong narrow-line region contribution to $H\beta$. A velocity shift is allowed between the components to account for the asymmetry of the line profile. The two Gaussian components do not necessarily have any physical significance, but are required to fit the line well enough to determine a reliable FWHM. The initial parameters are set such that the power-law continuum dominates the emission, but the FeII and the host galaxy can contribute when necessary. Fig. 1 shows examples of our fitting results. For details about the fitting procedure, see Shang et al. (2005).

In order to estimate black hole masses, we utilize the FWHM of the $H\beta$ line and the 5100 Å continuum flux determined by the fitting routine. The FWHM of the $H\beta$ line is computed numerically from the sum of the two Gaussian components used to fit the line. The largest source of uncertainty related to determining the FWHM is associated with the placement of the continuum, and we estimate typical uncertainties of 10–20%. The continuum luminosity is obtained from the power-law component flux value at rest-frame 5100 Å.

The bolometric luminosity is estimated as $L_{\text{bol}} = 9 \times \lambda L_{\lambda 5100}$. The Eddington luminosity is calculated as $L_{\text{Edd}} = 1.51 \times 10^{38} M_{\text{BH}}/M_{\odot} \text{ ergs s}^{-1}$ (Krolik 1998)², and the Ed-

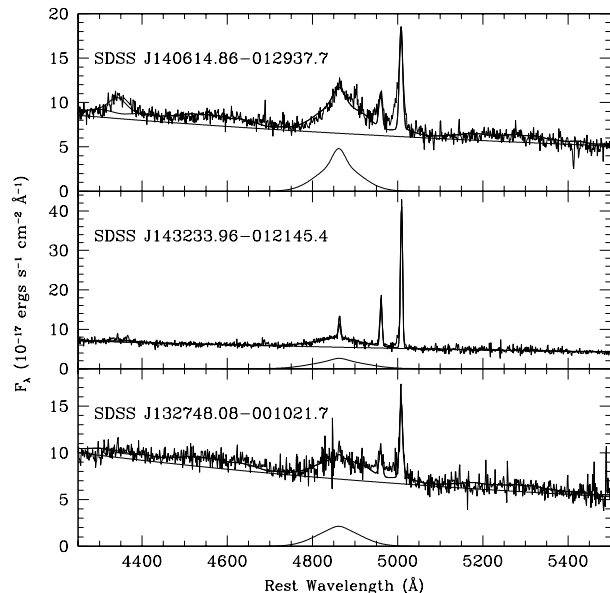


Figure 1. Three examples of SDSS spectra and typical fits to the $H\beta$ region used to make measurements of the line width and continuum flux needed for black hole mass estimation. Total, continuum, and line components are shown.

dington ratio as $\eta = L_{\text{bol}}/L_{\text{Edd}}$. Black hole masses, bolometric luminosities and Eddington ratios are listed in Table 1 for every quasar in the sample, and plotted as a function of redshift in Fig. 2 to illustrate the parameter space explored by the sample.

2.3 Variability Data

The QUEST1 Variability survey provides light curves for nearly 200,000 objects in B , V and R filters over a 2.4° wide strip centered at declination -1° and covering the range 10^{h} to $15^{\text{h}}30^{\text{min}}$ in right ascension (Rengstorf et al. 2004b). All sources in the 200k Light Curve Catalogue overlap with sources in the SDSS DR2. The limiting magnitudes of the 200k Light Curve Catalogue are $B \approx 19.6$, $V \approx 19.8$ and $R \approx 20.8$, and only point sources are included (typical seeing is $2''.8$). The QUEST1 light curves are given in terms of Julian date, instrumental magnitude and magnitude uncertainty in four filters denoted b , v , r_1 and r_3 (lower case used for instrumental magnitudes). In order to check for self-consistency, the QUEST1 survey uses two R filters, denoted r_1 and r_3 , hence a criterion for inclusion in the 200k catalogue is that the object has a significant detection in both R filters. Our matched sample therefore contains 104 quasars detected in each of the two R filters. In the V -filter we found 70 matches, whereas in the B -filter, only 11. Since a sample of 11 is too small for the purposes of this paper, we have ignored the B -band light curves. We have also ignored the

² Krolik (1998) derives the Eddington luminosity using a reduced particle mass, while other authors, e.g. Peterson (1997), use the proton mass. This changes the coefficient in the formula for Eddington luminosity from 1.51 to 1.26. Our analysis and conclusions do not depend on this coefficient

² Krolik (1998) derives the Eddington luminosity using a reduced particle mass, while other authors, e.g. Peterson (1997), use the

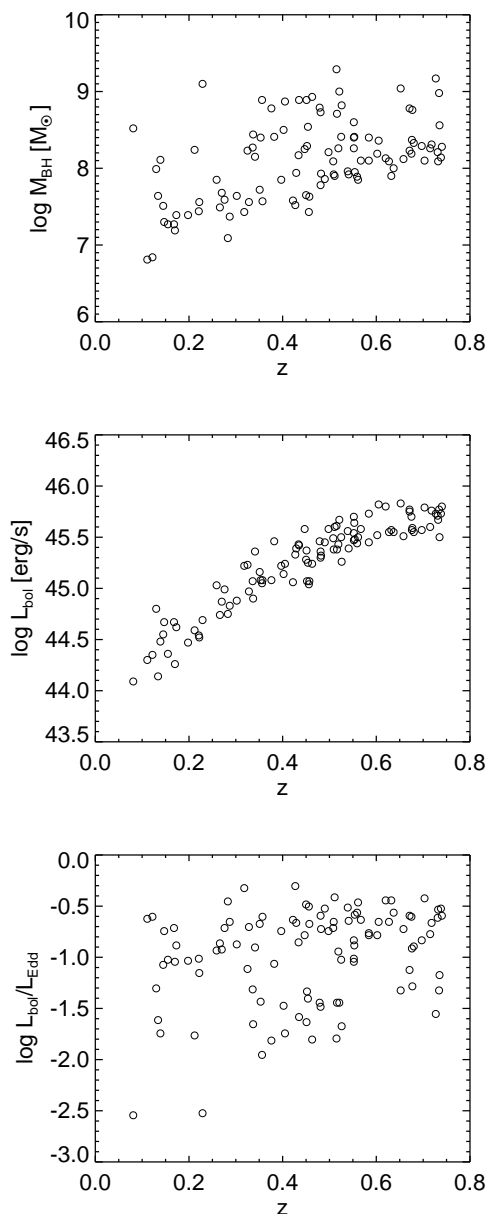


Figure 2. Plots of three fundamental AGN properties against redshift for the SDSS-QUEST1 sample.

r_1 measurements, and chosen r_3 for our analysis since the results for the two R -filters are very similar.

The QUEST1 Variability Survey extended over a period of 26 months, hence covers observed timescales ranging from a few hours up to 26 months. The time elapsed between two photometric measurements in the rest-frame of the quasars, referred to as the “time lag”, τ , scales with $(1+z)^{-1}$. The distribution of rest frame time lags for the 104 quasars in our matched sample is shown in Fig. 3. The majority of the measurements are concentrated in two regions, one at $0.5 < \tau < 30$ days and the other at $180 < \tau < 700$ days, with a gap around 100 days. The sample therefore probes variations on rest-frame timescales between ≈ 12 hrs up to one month, and between six months up to almost two years.

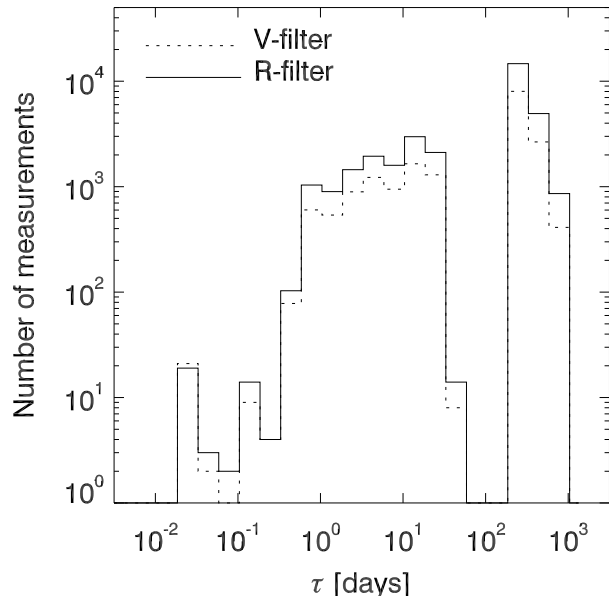


Figure 3. The distribution of rest-frame time lags for the SDSS-QUEST1 sample. The total number of objects in the R -filter is $N = 104$, and in V , $N = 70$.

The measurements extend all the way down to time lags of < 1 hr, but only for a few objects.

2.4 Measurements of Variability

2.4.1 Statistical Measurements

Variability can be characterized in several different ways, and we have chosen quantities describing both the variability of each quasar and the variability for the sample as a whole. Common for both of these is that the distribution of all possible magnitude differences (or variability amplitudes) on each light curve is evaluated, i.e.

$$\Delta m_{ij} = m_i - m_j, \quad (1)$$

where $i < j$. A light curve with N photometric measurements at different time lags therefore has $N(N-1)/2$ different variability amplitudes. The variability of a single quasar can be described by the standard deviation, mean, median and maximum of its distribution of variability amplitudes (see e.g. Giveon et al. 1999). We denote these quantities $\sigma_{\Delta m}$, $\langle \Delta m \rangle$, $\text{Med}(\Delta m)$ and $\text{Max}(\Delta m)$, and list them in Table 1 for both the V - and the R -filter. The standard deviation, $\sigma_{\Delta m}$, was evaluated by weighting each magnitude with the inverse of the uncertainty in the magnitude.

Also listed in Table 1, in the last column, is the variability global confidence level, denoted GCL, from the QUEST1 Variability catalogue. It is defined by Rengstorf et al. (2004b) as a weighted average of the variability confidence levels in every filter the source was detected, and indicates the percentage probability that a source is not variable purely by random fluctuations. The mean and median GCL of our matched sample is 79 and 88, respectively, and the percentage of objects with $\text{GCL} > 85$, which Rengstorf et al. (2004a) choose for spectroscopic follow-up and classify as

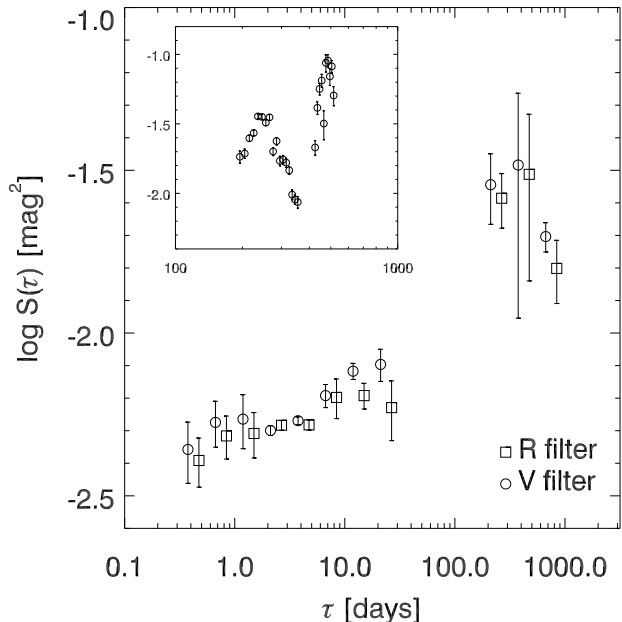


Figure 4. Structure functions for the whole sample in both *R*- and *V*-filter. The smaller inlaid figure shows the structure function in bins of 10 days at time lags between 100 and ≈ 700 days.

“highly variable”, is 58. Hence more than half of our sample contains highly variable objects, reflecting the fact that most quasars are indeed variable at some level.

2.4.2 Structure Functions

The variability measurements outlined in the previous section characterize how strongly variable each source is across the full light curve, but do not describe how the variability changes as a function of time lag. In order to investigate the time dependence of the variability, we utilize the first-order structure function, defined as

$$S(\tau) = \langle [m(t) - m(t + \tau)]^2 \rangle \quad (2)$$

(Hughes, Aller & Aller 1992), where $m(t)$ is the magnitude at time t , τ is the rest-frame time lag, and the $\langle \rangle$ brackets denote the ensemble average. In practice, the structure function is the sample average of all magnitude differences at a given time lag, τ . It is often used to characterize quasar variability (Hughes et al. 1992; Vanden Berk et al. 2004; de Vries et al. 2005) and is less sensitive to aliasing problems and gaps in the data than e.g. Fourier analysis. We evaluate the structure function for the sample within fixed logarithmic intervals of width 0.25 in $\log \tau$. The resulting structure function in both *V*- and *R*-filter is shown in Fig. 4 where only bins with more than 50 measurements have been included (the number of measurements per bin can be read off Fig. 3). The uncertainty in $S(\tau)$ at each $\log \tau$ interval was evaluated by splitting each bin in four equal parts and calculating the difference between $S(\tau)$ in each sub-bin and $S(\tau)$ in the full bin.

The behaviour of the structure function in Fig. 4 is typical for measurements where there is variability due to measurement noise at shorter time lags and variability intrinsic

to the source at longer time lags. For measurement noise, the correlation timescale is zero, hence the plateau at short time lags, $\tau \lesssim 5$ days, is characteristic of the photometric uncertainty in the data, here seen to be ≈ 0.05 – 0.06 mag. Since the plateau at short time lags merely probes the noise, we expect the structure function to be similar in both *V* and *R* in this region, which is indeed observed. For time lags $\gtrsim 6$ – 7 days, the structure function starts to increase. The increase is seen in both *V* and *R*, but with the sample being more variable in the *V*-filter. This is in line with previous observations, finding that quasars are more variable in the blue.

At time lags between one and six months there are no data, but at $\tau \gtrsim 6$ months, the structure function has increased significantly above the noise plateau. A structure function that increases from the noise plateau and levels off at longer time lags is typical of a process which has one characteristic, physically meaningful, timescale (Hughes et al. 1992). Whether there is such a plateau at longer timescales in our sample is difficult to determine because there are not enough measurements at long time lags (only three data points at $\log \tau > 2$). A leveling off at $\tau \approx 200$ days would indicate that there is a preferred timescale of roughly 200 days for the outbursts causing the variability, whereas a continued increase indicates that processes of many different timescales contribute to the variability.

It is uncertain whether the turn-over of the structure function at $\tau \approx 300$ – 400 days reflects a real change. Most likely it is caused by incompleteness or selection effects. Each bin, apart from the first and the last, contains measurements from all objects in the sample. The bin at the longest time lag contains objects that are biased toward smaller redshifts, because only for those can we probe the longest time lags. The smaller plot in the upper left-hand corner of Fig. 4 shows the structure function evaluated in bins of 10 days. There is a dip around $\tau \approx 400$ days, causing the larger error bar in the more coarsely binned data. The dip at ≈ 400 days, as well as the decrease in $S(\tau)$ at longer time lags may therefore be due to a bias introduced by incomplete sampling of time lags at the end of the one- and two-year periods in the QUEST1 variability survey. As the longest time sampling is obtained for the lower-redshift sources, and if the lower-redshift sources are biased toward lower variability, this could explain the drop in the structure function. It is well known that quasar variability continues to increase at time lags of the order several years (Hook et al. 1994; Vanden Berk et al. 2004; de Vries et al. 2005), hence the most likely explanation for the turn-over in this set of data is insufficient sampling at long time lags. A similar turn-over is also seen in the structure function analysis made by Rengstorf et al. (2006) on a sample of ~ 1000 QUEST1 quasars.

Regardless of the behaviour of the structure function in the longer time lag bin, the slope at the rising part is a meaningful parameter as it indicates the nature of the process causing the variability (Hughes et al. 1992). But as there is a gap in the data at time lags from one to six months, we can only estimate a lower limit to the slope. Fitting a straight line through the data points at $\tau > 6$ days gives a slope of 0.42 in *V* and 0.41 in *R*. This agrees very well with the slope of 0.41 ± 0.07 derived by Rengstorf et al. (2006) for their sample of roughly 1000 QUEST1 quasars.

Table 1. The total sample of 104 quasars with variability measurements and AGN parameters. The columns are (1) Sloan ID number, (2) redshift, (3) apparent Sloan r magnitude, (4) absolute magnitude in Sloan i -filter, (5)–(8) weighted standard deviation, mean, median and maximum of the distribution of variability amplitudes in the R -filter (units of magnitudes), (9)–(12) same as columns (5)–(8), but for the V -filter, (13) log of black hole mass in units of solar masses, (14) log of bolometric luminosity in units of ergs s^{-1} , (15) log of Eddington ratio, defined as $L_{\text{bol}}/L_{\text{Edd}}$, and (16) the global confidence level of variability as defined by Rengstorf et al. (2004b).

SloanID (SDSS J)	z	m_r	M_i	$\sigma_{\Delta R}$	$\langle \Delta R \rangle$	Med(ΔR)	Max(ΔR)	$\sigma_{\Delta V}$	$\langle \Delta V \rangle$	Med(ΔV)	Max(ΔV)	$\log M_{\text{BH}}$	$\log L_{\text{bol}}$	$\log \eta$	GCL
(1)	(2)	(3)	(4)	(5)	(6)	(7)	(8)	(9)	(10)	(11)	(12)	(13)	(14)	(15)	(16)
100110.52–004049.1	0.134	18.59	–20.31	0.060	0.073	0.057	0.310	0.063	0.071	0.070	0.207	7.640	44.14	–1.61	75.42
100215.83–001056.1	0.353	18.80	–22.51	0.083	0.098	0.087	0.295	0.101	0.115	0.105	0.358	8.400	45.08	–1.43	71.77
101003.14–001332.1	0.732	18.58	–24.42	0.079	0.104	0.089	0.420	0.083	0.107	0.095	0.347	8.090	45.67	–0.53	66.77
101658.66–000708.4	0.337	18.92	–22.34	0.301	0.262	0.156	0.809	0.000	0.000	0.000	0.000	8.440	44.90	–1.65	100.00
102504.34–004618.9	0.552	18.66	–23.96	0.103	0.131	0.079	0.358	0.125	0.147	0.099	0.436	8.260	45.54	–0.83	94.16
102522.66–001552.4	0.452	19.57	–22.71	0.091	0.102	0.086	0.361	0.000	0.000	0.000	0.000	8.290	45.07	–1.33	79.43
102606.73–005038.9	0.283	18.79	–22.03	0.155	0.191	0.199	0.502	0.000	0.000	0.000	0.000	7.090	44.75	–0.45	100.00
102920.70–004747.6	0.259	18.29	–22.45	0.040	0.050	0.046	0.141	0.070	0.088	0.069	0.291	7.850	45.03	–0.93	98.36
102926.13–002643.3	0.198	18.91	–21.51	0.062	0.079	0.075	0.250	0.000	0.000	0.000	0.000	7.390	44.47	–1.03	34.60
103031.41–001902.7	0.561	19.21	–23.38	0.159	0.180	0.170	0.461	0.181	0.213	0.189	0.588	7.850	45.50	–0.46	80.74
103222.57–000345.6	0.559	19.31	–23.25	0.103	0.123	0.102	0.386	0.075	0.087	0.079	0.281	7.890	45.44	–0.56	69.38
103703.10–001854.9	0.287	19.13	–21.98	0.069	0.085	0.083	0.253	0.000	0.000	0.000	0.000	7.370	44.83	–0.65	39.01
104122.84–005618.4	0.498	18.54	–23.69	0.043	0.051	0.043	0.167	0.033	0.039	0.034	0.098	8.210	45.58	–0.74	71.06
104733.39–004700.5	0.740	18.46	–24.44	0.041	0.049	0.044	0.157	0.046	0.055	0.047	0.208	8.280	45.80	–0.59	48.56
105336.71–001727.3	0.482	19.19	–23.00	0.056	0.069	0.062	0.216	0.068	0.078	0.069	0.241	7.930	45.32	–0.72	40.50
105342.21–001420.1	0.676	19.13	–23.76	0.060	0.068	0.061	0.206	0.070	0.072	0.063	0.245	8.370	45.57	–0.91	37.58
105606.93–004655.5	0.336	19.06	–22.24	0.061	0.074	0.058	0.337	0.069	0.077	0.064	0.277	8.270	45.07	–1.31	52.13
105932.52–004354.8	0.155	18.76	–20.91	0.056	0.065	0.057	0.199	0.058	0.073	0.067	0.244	7.270	44.36	–1.02	30.09
110054.14–005038.4	0.541	19.39	–23.22	0.064	0.080	0.072	0.220	0.000	0.000	0.000	0.000	7.920	45.39	–0.64	36.58
111456.02–004019.2	0.734	19.01	–24.04	0.095	0.119	0.121	0.371	0.081	0.106	0.090	0.367	8.980	45.77	–1.32	96.39
111756.85–000220.5	0.457	19.24	–22.78	0.065	0.080	0.072	0.236	0.000	0.000	0.000	0.000	7.630	45.07	–0.67	48.17
112646.43–013417.9	0.341	18.55	–22.74	0.052	0.062	0.055	0.227	0.086	0.096	0.087	0.307	8.150	45.36	–0.90	87.12
112747.54–015830.1	0.519	18.93	–23.48	0.064	0.081	0.071	0.232	0.084	0.100	0.091	0.315	8.260	45.43	–0.94	33.88
113140.63–015118.3	0.434	19.13	–22.88	0.231	0.235	0.121	0.611	0.000	0.000	0.000	0.000	8.170	45.43	–0.85	100.00
113318.89–004112.0	0.511	18.66	–23.80	0.052	0.064	0.058	0.196	0.045	0.052	0.047	0.140	7.900	45.60	–0.41	46.10
113416.81–001902.4	0.356	18.95	–22.60	0.118	0.142	0.126	0.370	0.000	0.000	0.000	0.000	8.890	45.05	–1.95	100.00
113607.51–012313.7	0.266	18.96	–21.84	0.093	0.102	0.086	0.384	0.000	0.000	0.000	0.000	7.490	44.74	–0.86	98.18
114455.78–002142.7	0.351	18.52	–22.85	0.152	0.160	0.128	0.455	0.127	0.151	0.139	0.446	7.720	45.16	–0.67	100.00
114528.56–004739.0	0.715	19.01	–23.99	0.065	0.085	0.072	0.261	0.000	0.000	0.000	0.000	8.260	45.60	–0.77	63.05
114718.05–013206.9	0.382	18.11	–23.41	0.048	0.059	0.050	0.225	0.066	0.078	0.067	0.239	8.410	45.46	–1.06	86.87
114758.38–001551.8	0.718	18.95	–24.12	0.085	0.114	0.094	0.375	0.068	0.083	0.073	0.261	8.310	45.76	–0.66	44.69
114916.75–004231.8	0.735	18.82	–24.15	0.132	0.186	0.162	0.582	0.103	0.127	0.142	0.331	8.560	45.50	–1.17	97.57
115156.69–011800.6	0.170	18.89	–21.01	0.068	0.079	0.070	0.256	0.000	0.000	0.000	0.000	7.190	44.26	–1.04	33.67
115216.12–005352.1	0.637	18.85	–24.00	0.051	0.064	0.050	0.288	0.034	0.044	0.040	0.131	8.000	45.55	–0.56	29.37
115306.94–004512.7	0.357	19.04	–22.28	0.066	0.076	0.068	0.228	0.063	0.071	0.062	0.186	7.570	45.08	–0.60	52.34
115342.99–001159.8	0.602	18.74	–23.94	0.082	0.097	0.085	0.302	0.091	0.107	0.100	0.305	8.190	45.52	–0.78	94.59
120553.64–004651.0	0.671	18.47	–24.48	0.050	0.058	0.049	0.202	0.059	0.072	0.084	0.189	8.230	45.75	–0.59	87.97
120619.01–003959.5	0.675	18.59	–24.14	0.087	0.102	0.095	0.279	0.060	0.070	0.061	0.207	8.190	45.70	–0.60	82.36
120629.59–004831.2	0.463	19.30	–23.04	0.111	0.127	0.109	0.453	0.131	0.159	0.138	0.421	8.930	45.24	–1.80	99.95
120644.82–012737.1	0.509	18.79	–23.56	0.098	0.122	0.104	0.339	0.127	0.150	0.131	0.383	7.920	45.38	–0.65	100.00

Table 1 – continued

SloanID (SDSS J) (1)	z (2)	m_r (3)	M_i (4)	$\sigma_{\Delta R}$ (5)	$\langle \Delta R \rangle$ (6)	Med(ΔR) (7)	Max(ΔR) (8)	$\sigma_{\Delta V}$ (9)	$\langle \Delta V \rangle$ (10)	Med(ΔV) (11)	Max(ΔV) (12)	$\log M_{\text{BH}}$ (13)	$\log L_{\text{bol}}$ (14)	$\log \eta$ (15)	GCL (16)
120708.57–013614.0	0.620	18.11	−24.72	0.082	0.099	0.085	0.273	0.090	0.106	0.097	0.300	8.130	45.80	−0.44	78.80
120806.89–013509.7	0.481	18.89	−23.20	0.051	0.061	0.052	0.191	0.069	0.084	0.075	0.274	7.780	45.30	−0.59	49.12
121224.35–015246.3	0.429	18.84	−23.14	0.075	0.090	0.078	0.293	0.095	0.098	0.075	0.331	7.940	45.39	−0.66	79.92
121337.06–000047.1	0.454	18.85	−23.25	0.092	0.117	0.104	0.451	0.098	0.118	0.102	0.379	8.540	45.25	−1.40	87.49
121449.89–011245.0	0.671	18.32	−24.67	0.039	0.046	0.038	0.140	0.046	0.055	0.049	0.194	8.780	45.77	−1.12	45.01
121747.38–015048.6	0.652	18.77	−24.12	0.169	0.195	0.191	0.560	0.188	0.208	0.181	0.521	9.040	45.83	−1.32	100.00
122015.70–000251.6	0.397	19.05	−22.68	0.101	0.118	0.114	0.362	0.097	0.116	0.101	0.318	7.850	45.22	−0.74	92.07
122032.96–001434.1	0.212	18.81	−21.75	0.075	0.081	0.069	0.306	0.000	0.000	0.000	0.000	8.240	44.59	−1.76	84.62
122617.38–015955.3	0.584	18.90	−23.79	0.095	0.119	0.101	0.414	0.000	0.000	0.000	0.000	8.100	45.45	−0.76	99.18
123246.62–013639.9	0.325	17.75	−23.11	0.053	0.065	0.054	0.181	0.115	0.134	0.122	0.358	8.230	45.23	−1.11	100.00
122347.96–013303.9	0.508	19.11	−23.34	0.105	0.129	0.114	0.371	0.112	0.136	0.137	0.410	8.090	45.49	−0.71	100.00
122727.47–012158.2	0.456	19.37	−22.86	0.105	0.126	0.103	0.492	0.133	0.169	0.150	0.511	7.430	45.04	−0.50	99.74
123452.49–015955.6	0.328	18.78	−22.30	0.108	0.125	0.112	0.392	0.000	0.000	0.000	0.000	7.560	44.97	−0.70	100.00
124519.73–005230.4	0.221	18.88	−21.74	0.038	0.049	0.030	0.188	0.000	0.000	0.000	0.000	7.440	44.54	−1.01	14.76
125055.28–015556.8	0.081	17.83	−20.43	0.031	0.038	0.033	0.131	0.050	0.059	0.051	0.222	8.520	44.09	−2.54	57.53
125337.35–004809.6	0.427	18.47	−23.27	0.044	0.055	0.047	0.210	0.057	0.066	0.058	0.241	7.520	45.33	−0.30	66.08
125952.49–015707.2	0.447	18.17	−23.86	0.070	0.082	0.054	0.238	0.071	0.084	0.058	0.289	8.250	45.58	−0.78	99.79
130023.21–005429.7	0.122	17.62	−21.59	0.062	0.067	0.051	0.218	0.062	0.072	0.046	0.250	6.840	44.35	−0.60	100.00
130610.05–011600.6	0.229	18.47	−22.04	0.108	0.133	0.116	0.319	0.000	0.000	0.000	0.000	9.100	44.69	−2.52	100.00
130725.69–004525.7	0.490	18.79	−23.49	0.054	0.076	0.067	0.258	0.052	0.058	0.046	0.176	7.860	45.45	−0.52	40.16
130707.70–002542.8	0.450	18.85	−23.24	0.086	0.110	0.096	0.328	0.116	0.142	0.118	0.471	7.650	45.28	−0.48	97.41
130845.68–013053.9	0.111	17.65	−21.35	0.054	0.066	0.055	0.223	0.069	0.081	0.075	0.249	6.810	44.30	−0.62	100.00
130916.67–001550.1	0.422	19.15	−22.66	0.095	0.123	0.106	0.370	0.000	0.000	0.000	0.000	7.580	45.06	−0.63	97.18
130937.34–014950.4	0.703	18.42	−24.56	0.089	0.103	0.093	0.360	0.098	0.127	0.115	0.423	8.100	45.79	−0.42	100.00
132231.12–001124.6	0.173	18.20	−21.77	0.058	0.065	0.062	0.224	0.074	0.090	0.075	0.360	7.390	44.62	−0.88	94.38
132514.79–012132.3	0.553	18.65	−24.04	0.179	0.207	0.189	0.514	0.000	0.000	0.000	0.000	8.410	45.64	−0.88	100.00
132704.54–003627.5	0.302	19.10	−21.95	0.070	0.087	0.068	0.376	0.000	0.000	0.000	0.000	7.640	44.88	−0.87	71.27
132705.88–012415.5	0.168	17.71	−22.21	0.048	0.057	0.041	0.269	0.064	0.079	0.069	0.244	7.270	44.67	−0.71	99.95
132748.08–001021.7	0.479	18.97	−23.30	0.125	0.140	0.110	0.494	0.000	0.000	0.000	0.000	8.790	45.46	−1.44	100.00
133105.30–005731.8	0.526	19.30	−23.21	0.060	0.077	0.065	0.280	0.000	0.000	0.000	0.000	8.820	45.26	−1.67	49.11
133141.02–015212.4	0.145	18.37	−21.26	0.088	0.101	0.089	0.285	0.103	0.114	0.082	0.257	7.510	44.55	−1.07	98.12
133350.26–003946.9	0.727	18.67	−24.36	0.047	0.053	0.044	0.210	0.059	0.072	0.065	0.205	9.170	45.73	−1.55	43.21
133806.59–012412.8	0.451	19.05	−23.14	0.172	0.206	0.192	0.505	0.000	0.000	0.000	0.000	8.890	45.37	−1.63	100.00
134233.70–001148.0	0.516	19.13	−23.24	0.070	0.086	0.072	0.364	0.078	0.100	0.086	0.342	8.710	45.38	−1.44	28.95
134318.45–005933.6	0.697	18.75	−24.26	0.173	0.182	0.140	0.550	0.145	0.172	0.138	0.581	8.290	45.57	−0.83	100.00
134354.19–012759.1	0.731	18.60	−24.46	0.052	0.063	0.052	0.231	0.000	0.000	0.000	0.000	8.210	45.71	−0.61	81.53
134818.25–002441.9	0.738	18.62	−24.54	0.068	0.079	0.062	0.290	0.072	0.088	0.075	0.353	8.140	45.73	−0.52	71.63
135028.88–012958.1	0.677	19.25	−23.75	0.103	0.131	0.107	0.517	0.127	0.145	0.132	0.498	8.760	45.59	−1.28	100.00
135727.37–012639.9	0.147	17.85	−21.81	0.035	0.045	0.040	0.157	0.061	0.074	0.060	0.261	7.300	44.67	−0.74	98.91
135830.46–012255.7	0.658	18.95	−24.00	0.070	0.084	0.073	0.273	0.000	0.000	0.000	0.000	8.120	45.51	−0.72	57.49
140025.53–012957.0	0.584	18.46	−24.30	0.044	0.052	0.045	0.159	0.045	0.056	0.047	0.226	8.400	45.73	−0.78	69.77
140252.06–015258.1	0.402	19.14	−22.69	0.079	0.099	0.087	0.334	0.000	0.000	0.000	0.000	8.500	45.14	−1.47	99.65
142526.50–004421.5	0.567	19.14	−23.64	0.061	0.071	0.065	0.253	0.000	0.000	0.000	0.000	8.100	45.58	−0.63	76.31
140614.86–012937.7	0.552	18.52	−24.06	0.059	0.074	0.066	0.237	0.067	0.082	0.075	0.266	8.600	45.70	−1.01	99.98

Table 1 – *continued*

SloanID (SDSS J) (1)	z (2)	m_r (3)	M_i (4)	$\sigma_{\Delta R}$ (5)	$\langle \Delta R \rangle$ (6)	Med(ΔR) (7)	Max(ΔR) (8)	$\sigma_{\Delta V}$ (9)	$\langle \Delta V \rangle$ (10)	Med(ΔV) (11)	Max(ΔV) (12)	$\log M_{\text{BH}}$ (13)	$\log L_{\text{bol}}$ (14)	$\log \eta$ (15)	GCL (16)
140923.51–012430.5	0.405	19.14	−22.71	0.158	0.155	0.108	0.476	0.000	0.000	0.000	0.000	8.870	45.24	−1.74	100.00
141238.77–012033.9	0.139	18.25	−21.37	0.053	0.065	0.055	0.196	0.069	0.081	0.069	0.242	8.110	44.48	−1.74	95.42
141638.18–005352.9	0.552	18.71	−23.78	0.179	0.191	0.140	0.604	0.197	0.235	0.226	0.686	8.400	45.47	−1.04	100.00
141647.59–012657.4	0.376	19.30	−22.36	0.113	0.151	0.117	0.489	0.000	0.000	0.000	0.000	8.780	45.08	−1.81	99.99
141949.83–000643.7	0.515	18.91	−23.48	0.137	0.177	0.102	0.614	0.108	0.143	0.087	0.602	9.290	45.61	−1.79	100.00
142352.01–000705.2	0.680	18.89	−23.90	0.089	0.112	0.090	0.388	0.099	0.118	0.095	0.421	8.330	45.55	−0.89	84.43
142441.20–000727.1	0.318	18.13	−22.86	0.050	0.060	0.052	0.242	0.072	0.086	0.072	0.297	7.430	45.22	−0.32	76.20
142726.64–001950.0	0.222	18.86	−21.85	0.184	0.217	0.184	0.569	0.000	0.000	0.000	0.000	7.560	44.52	−1.15	100.00
143233.96–012145.4	0.521	18.95	−23.65	0.114	0.125	0.109	0.367	0.140	0.159	0.141	0.467	9.000	45.67	−1.44	100.00
143306.57–012922.9	0.627	19.09	−23.66	0.111	0.133	0.115	0.453	0.114	0.129	0.112	0.417	8.090	45.55	−0.65	100.00
145704.63–012253.0	0.525	18.67	−23.70	0.122	0.158	0.136	0.551	0.139	0.172	0.140	0.607	8.410	45.50	−1.02	100.00
145857.84–013419.3	0.276	18.59	−22.23	0.044	0.053	0.048	0.167	0.081	0.101	0.084	0.379	7.590	44.99	−0.71	86.43
145859.95–001504.3	0.481	18.73	−23.56	0.106	0.135	0.107	0.394	0.157	0.193	0.152	0.555	8.730	45.36	−1.48	99.90
145925.04–015650.0	0.539	18.76	−23.65	0.098	0.118	0.095	0.600	0.000	0.000	0.000	0.000	7.960	45.56	−0.51	99.99
151538.94–001240.8	0.435	19.15	−22.97	0.053	0.065	0.055	0.234	0.000	0.000	0.000	0.000	8.890	45.42	−1.58	58.49
151750.63–015534.6	0.554	19.01	−23.68	0.103	0.128	0.110	0.361	0.000	0.000	0.000	0.000	7.950	45.48	−0.58	100.00
152018.65–015037.4	0.632	18.99	−23.92	0.078	0.089	0.083	0.283	0.000	0.000	0.000	0.000	7.900	45.57	−0.44	72.81
152035.34–002040.1	0.130	17.17	−22.33	0.051	0.064	0.052	0.249	0.041	0.048	0.037	0.226	7.990	44.80	−1.30	83.43
152809.55–000044.9	0.605	18.07	−24.82	0.068	0.081	0.074	0.237	0.085	0.098	0.088	0.321	8.360	45.82	−0.65	100.00
152942.75–015934.0	0.270	19.06	−21.84	0.073	0.087	0.079	0.265	0.000	0.000	0.000	0.000	7.680	44.87	−0.92	96.63

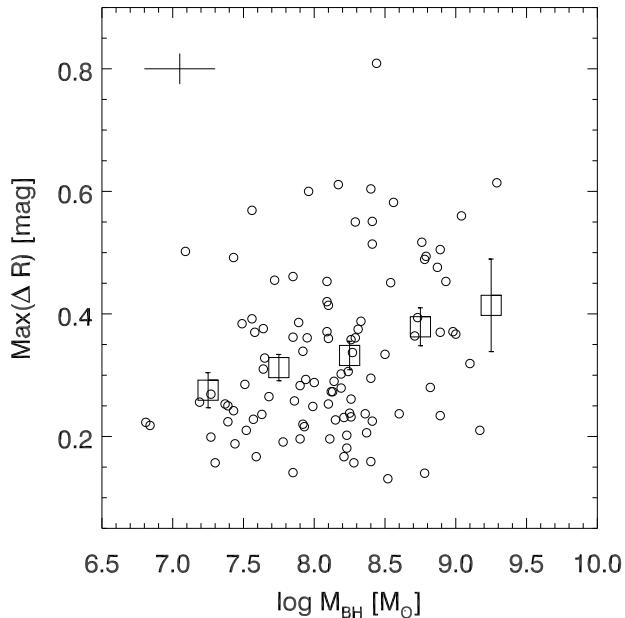


Figure 5. The maximum variability amplitude in the R -filter as a function of black hole mass. Overplotted with open squares are the mean $\text{Max}(\Delta R)$ in five black hole mass bins with the error bars signifying the error in the mean. The cross in the upper left-hand corner indicates a typical error bar for the open circles.

3 ANALYSIS

3.1 Variability–black hole mass correlation

In order to investigate whether quasar variability correlates with any of the AGN parameters black hole mass, bolometric luminosity or the Eddington ratio, we calculated Pearson correlation coefficients. First of all, we note that there exists a number of strong but uninteresting correlations in the complete correlation matrix that reflect known selection effects in flux-limited quasar samples (e.g., the increase in luminosity with redshift). Secondly, we also measure significant correlations between quasar variability amplitude and black hole mass. The correlation coefficients for the most interesting parameters are shown in Table 2. The strongest correlation is that between variability as measured in terms of $\text{Max}(\Delta R)$ (i.e. maximum variability amplitude) and black hole mass. The correlation coefficient is 0.285, which corresponds to a Student’s t -statistic of 3.0 and a two-sided probability of arising by chance of 0.3%. The correlation between variability amplitude and black hole mass is therefore present at the $\approx 3\sigma$ level. Other measures of variability have qualitatively similar, but somewhat less significant, correlations with black hole mass. Fig. 5 shows the maximum variability amplitude as a function of black hole mass. There is not a clear linear relationship, but it is evident that the sources displaying the most variability have, on average, higher black hole masses. We also evaluated the correlation matrix using the variability parameters as determined in the V -filter, and obtain very similar results to the R -filter.

Further support for the correlation between variability amplitude and black hole mass is provided by additional analysis of the structure function. For each filter, we com-

Table 2. Pearson correlation coefficients between variability parameters and the AGN parameters black hole mass, bolometric luminosity and Eddington ratio, η . Two-sided probabilities, P , that the correlations have arisen by chance are given immediately under each row of correlation coefficients, and were calculated based on the Student’s t -statistic.

Variability	$\log M_{\text{BH}}$	$\log L_{\text{bol}}$	$\log \eta$
$\sigma_{\Delta R}$	0.248	0.102	−0.188
P	0.011	0.303	0.057
$\langle \Delta R \rangle$	0.273	0.137	−0.184
P	0.005	0.164	0.062
$\text{Med}(\Delta R)$	0.229	0.142	−0.129
P	0.019	0.150	0.193
$\text{Max}(\Delta R)$	0.285	0.146	−0.189
P	0.003	0.139	0.055
GCL	0.126	0.032	−0.114
P	0.203	0.746	0.250

pute the structure function for two different bins in rest-frame time lag (1–100 and > 100 days), with each time lag bin separated into several smaller bins of black hole mass. This allows us to investigate variability as a function of both rest-frame time lag and black hole mass. We find a significantly rising trend of variability with black hole mass, see the left-hand panel of Fig. 6. In this figure, it can also be seen that the main contribution to the variability–black hole mass correlation comes from the longer time lags at $\tau > 100$ days. At shorter time lags the correlation is probably diluted by random measurement noise which is not expected to correlate with AGN properties.

3.2 Correlations with redshift and bolometric luminosity

The middle panel of Fig. 6 shows quasar variability as a function of redshift, and it is clear that the known correlation between variability and redshift is present in our sample.

The last panel of Fig. 6 shows variability as a function of quasar bolometric luminosity, and this figure agrees with the result from the correlation analysis that there is no significant correlation present between variability and bolometric luminosity. We do however expect an anti-correlation between variability and quasar luminosity as brought up in the introduction, but the strong luminosity–redshift correlation in the sample counters it. This is supported by a partial Spearman correlation analysis revealing that $\text{Max}(\Delta R)$ and bolometric luminosity at constant redshift are anti-correlated with a partial Spearman’s correlation coefficient of -0.212 and a probability of 0.2% of the anti-correlation being caused by underlying correlations with redshift. The variability–luminosity anti-correlation is therefore detected in our sample when redshift effects are accounted for.

4 DISCUSSION

4.1 Selection effects

Could the correlation between variability and black hole mass be caused through more primary correlations with another variable? For instance, variability and redshift are

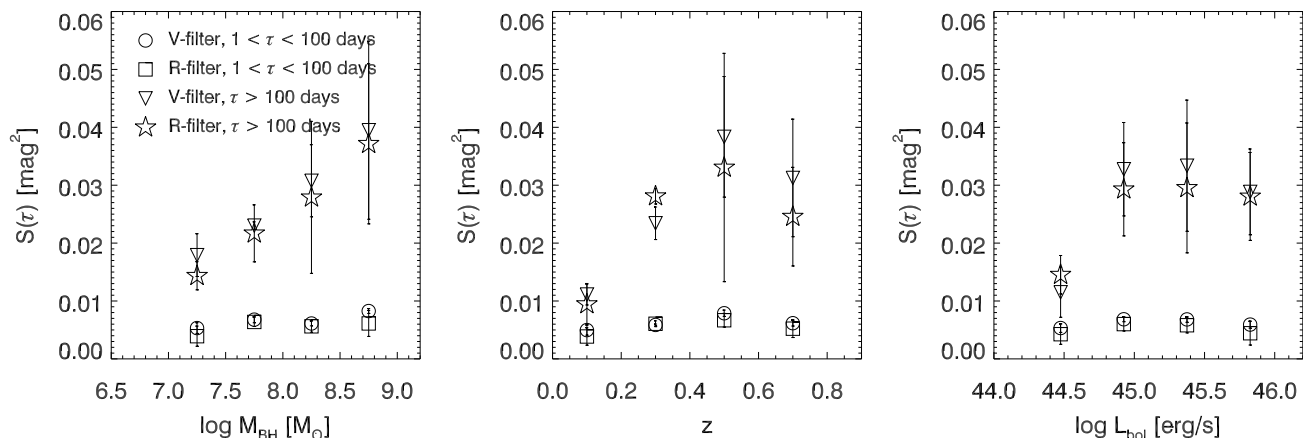


Figure 6. Structure functions in V and R as a function of black hole mass (left), redshift (centre) and bolometric luminosity (right). The increase in variability is clearly seen for higher black hole masses at longer time lags ($\tau > 100$ days).

known to be correlated, and Fig. 2 shows that black hole mass is indeed correlated with redshift in our sample (Spearman’s $\rho = 0.466$ with probability of correlation arising by chance 6×10^{-7}). As discussed in the introduction, the redshift–variability correlation comes about as a combination of the hardening (bluening) of quasar spectra in their brighter phases and the fact that a fixed passband in the observers frame probes progressively shorter rest-frame wavelengths at higher redshifts. Because higher-redshift quasars in flux-limited samples are sampled at bluer rest-frame wavelengths where they are more variable, a variability–redshift correlation emerges. This could imply that a bias with redshift causes the more massive black holes to be associated with stronger variability.

In order to check whether the variability–redshift correlation in the sample is causing the variability–black hole mass correlation, we evaluate Spearman’s partial correlation coefficient between black hole mass and variability amplitude, at constant redshift. We obtain $\rho_{\text{Max}(\Delta R)M,z} = 0.203$ with a probability of 0.0035 that the variability–black hole mass correlation is caused by underlying correlations with redshift. Hence the variability–black hole mass correlation does not appear to be caused by underlying correlations with redshift.

We also considered the possibility that the correlation could arise as a result of a more primary correlation with luminosity, because black hole mass is also correlated with bolometric luminosity in our sample ($\rho = 0.513$ with a probability of arising by chance of 2.6×10^{-8}). A partial Spearman correlation analysis shows that the correlation coefficient between $\text{Max}(\Delta R)$ and M_{BH} at constant L_{bol} is 0.254 with the probability of the correlation being caused by underlying correlations with L_{bol} being 2×10^{-4} .

Additional multivariate regression analysis and principle component analysis support the conclusions of the partial correlation analysis. When predicting the $\text{Max}(\Delta R)$ parameter based on both black hole mass and redshift, only black hole mass is significant, still at the two per cent level. There is thus no convincing evidence that the variability–black hole mass correlation is caused by simple selection effects.

4.2 Residual Host Galaxy Contamination

The lowest luminosity AGN in our SDSS-QUEST1 sample are Seyfert galaxies and their spectra may suffer from some level of host galaxy contamination despite our efforts to include a host galaxy component in the spectral fitting. Host galaxy contamination would occur preferentially for the lowest luminosity AGNs which are also those with the largest timescales sampled and tending to have smaller black hole masses. Two offsetting effects may occur: the stronger effect, depending linearly on the host-to-AGN ratio, dilutes the variability; the weaker effect, depending on the host-to-AGN ratio to the 0.7 power (Kaspi et al. 2000, 2005), overestimates the black hole mass.

In general we were conservative during the fitting and used zero initial host galaxy contribution with small steps, and only a few spectra required much host galaxy contribution. Furthermore, the QUEST1 variability catalogue does not include objects regarded as resolved, and only a few SDSS spectra display any clear host galaxy features. Finally, the trend between black hole mass and variability is still present within a sub-sample of higher luminosity quasars which are expected to be less affected by host galaxy contamination (Vanden Berk et al. 2006). Host galaxy contamination has however been noted to have significant effects on measurements of AGN luminosities in more luminous PG quasars (e.g. Bentz et al. 2006), so it is a potential concern. We conclude that even though host galaxy contamination could artificially enhance a variability amplitude–black hole mass correlation, it is a weak effect and unlikely to be important for our sample.

4.3 Physical models of quasar variability

Studies have shown that X-ray, UV and optical quasar flux variations are approximately simultaneous, supporting a model where reprocessing is essential. In this model, the optical and UV flux originate in an accretion disk which is irradiated by an X-ray variable disk corona. Short-timescale variations in this model are explained as either flares or variations in the optical depth of the corona. Longer timescale variations, on the order of months to years, may be related

to the propagation of the shorter-timescale variations (see Ulrich et al. 1997, and references therein). In summary, a number of models for quasar optical variability exists but there are no clear predictions relating variability amplitude and black hole mass.

There are predictions, however, of how different sources of optical variability can be associated with different characteristic timescales and many of these timescales depend on black hole mass. Collier & Peterson (2001) list several (light crossing time, accretion timescale, orbital timescale and accretion disk thermal timescale, see also Krolik (1998)), and attempt to define a relationship between black hole mass and characteristic variability timescale. Studying a sample of 10 well-monitored AGN, they report evidence of characteristic optical variability timescales correlating with black hole mass. The timescales they are studying range from a few weeks for AGN with black hole masses of $\sim 10^7 M_\odot$ to a few months for AGN with black hole masses of $\sim 10^8 M_\odot$, and are roughly consistent with accretion disk thermal timescales.

On timescales of a few weeks, the QUEST1 light curves are dominated by observational uncertainties, and timescales of several months are not well sampled. The QUEST1 time sampling is far from complete, essentially sampling timescales of weeks and 1–2 years, with little in between and nothing longer. The timescales that are well sampled, and which possess the most variability, are 1–2 years (also discussed by Rengstorf et al. 2006). AGN with black hole masses of $\sim 10^8 M_\odot$ to $\sim 10^9 M_\odot$, which we have in our sample, would be expected to have accretion disk thermal characteristic timescales on the order of 1–2 years. If the Collier & Peterson (2001) result is correct, we may be seeing a correlation resulting from the time sampling of QUEST1. If we are biased toward detecting intrinsic quasar variability only at longer timescales, i.e. > 100 days, and if there is a relation between characteristic variability timescale and black hole mass, we may be preferentially detecting strong variability in the AGN with higher black hole masses. The correlation we observe could therefore be a manifestation of the black hole mass dependence on AGN physical timescales.

There are three arguments against this: 1) The relation between characteristic variability timescales and black hole mass is highly speculative and not based on anything that has been well established yet. 2) The variability–black hole mass correlation is present also in the part of the sample having $M_{\text{BH}} > 10^8 M_\odot$, although with lower significance than for the complete sample. Hence the correlation is not formed solely by the presence of quasars at $M_{\text{BH}} < 10^8 M_\odot$ with variability amplitudes comparable to the noise level. 3) It is actually the lower redshift quasars (biased toward lower black hole masses) that have the best sampling of rest frame time lags over the time base line of the QUEST1 survey. The lower redshift quasars should therefore make a larger contribution to the structure function at intermediate to longer time lags as compared to the higher redshift ones. This effect would work in the opposite direction to what is expected due to the incomplete temporal sampling discussed above.

We therefore favour an explanation where the correlation we observe is due to a real relation between variability amplitude and black hole mass. However, as there are no models linking variability amplitude and black hole mass, it is difficult to explore this in more details at this stage. In

order to confirm the validity of a variability–black hole mass correlation, larger samples of quasars with better and more complete temporal sampling are needed.

Our ensemble structure functions do not show evidence for a characteristic timescale, although data at longer timescales are needed to confirm a turn-over or flattening in the structure function. As discussed in Section 2.4.2, the dips in the structure function at ≈ 400 and 700 days is caused by incomplete sampling of time lags at the end of the 1 and 2 year periods in the QUEST1 variability survey. The structure function at the end of each observing period will be biased toward lower-redshift quasars for which we can probe the longest rest frame time lags. As we are probably biased toward the lower-mass black holes at lower redshifts, the variability–black hole mass correlation could explain the drop in the structure function at longer time lags.

We also note that the variability–black hole mass correlation may help explain the result that radio-loud quasars are marginally more variable than radio-quiet. This follows if the most radio-loud objects selected from the top of the radio luminosity function are the ones with the more massive black holes (e.g. Lacy et al. 2001).

4.4 Palomar-Green (PG) Quasars

We note that good light curves and black hole masses of PG quasars are available in the literature. We were able to assemble a sample of 28 PG quasars with variability parameters from Giveon et al. (1999) and black hole masses from Vestergaard & Peterson (2006), and looked for corroboration of our SDSS-QUEST1 results. We found no significant correlations between variability and black hole mass for the PG quasars, possibly because of the smaller sample size. We did not add these data points to our SDSS-QUEST1 sample due to differences in parameter space and time sampling.

5 CONCLUSIONS

In this study we have matched a sample of broad-lined AGN at redshifts $z < 0.75$ from the SDSS (Abazajian et al. 2004) with sources in the 200k Light Curve Catalogue of the QUEST1 Variability Survey (Rengstorf et al. 2004b), yielding a total sample of 104 quasars. The Sloan spectra are used to estimate black hole masses from $H\beta$ linewidths and continuum luminosities at rest frame 5100 Å (Vestergaard & Peterson 2006). The light curves are used to evaluate the variability of each quasar in the sample, as well as the time-dependence on variability for the whole ensemble of quasars.

We conclude that there is evidence for a correlation between the black hole mass of a quasar and its variability properties. In particular, the variability amplitude tends to be larger with increasing black hole mass, a trend that is most pronounced for the larger timescales probed by the QUEST1 Variability Survey. The variability–black hole mass correlation does not appear to be caused by obvious selection effects, host galaxy contamination or correlations between variability and luminosity/redshift. We have also discussed whether the correlation may be a manifestation of a relation between black hole mass and accretion disk thermal time scale. This can come about if the temporal sampling in

the QUEST1 survey gives rise to a bias toward variability at longer time scales. There are however no convincing and established arguments supporting this explanation, hence we favour a scenario in which the more massive black holes have larger variability amplitudes.

The general robustness of the variability–black hole mass correlation should be confirmed with samples of similar, or larger, size consisting of objects possessing longer and better temporal sampling of the light curves. Improvements in technology and a growing recognition of the untapped power of time domain analysis promise to provide such data sets in the near future.

ACKNOWLEDGMENTS

MSB thanks the ESO Scientific Visitor Programme for support and hospitality, and the National Science Foundation for support through grant AST-0507781. The authors also thank the referee for comments which helped improve the presentation of this work. This research has made use of the NASA/IPAC Extragalactic Database (NED) which is operated by the Jet Propulsion Laboratory, California Institute of Technology, under contract with the National Aeronautics and Space Administration. We would like to thank those involved in making the Sloan Digital Sky Survey and the QUEST1 Variability Survey realities with public databases.

Funding for the SDSS and SDSS-II has been provided by the Alfred P. Sloan Foundation, the Participating Institutions, the National Science Foundation, the U.S. Department of Energy, the National Aeronautics and Space Administration, the Japanese Monbukagakusho, the Max Planck Society, and the Higher Education Funding Council for England. The SDSS Web Site is <http://www.sdss.org/>.

REFERENCES

- Abazajian K., et al. 2004, *AJ*, 128, 502
- Angione R. J., Smith H. J., 1972, in Evans D. S., Wills D., Wills B. J., eds, *IAU Symp. 44: External Galaxies and Quasi-Stellar Objects Optical Variability of Twenty-Two Quasi-Stellar Objects*. pp 171–+
- Aretxaga I., Cid Fernandes R., Terlevich R. J., 1997, *MNRAS*, 286, 271
- Aretxaga I., Terlevich R., 1994, *MNRAS*, 269, 462
- Bentz M. C., Peterson B. M., Pogge R. W., Vestergaard M., Onken C. A., 2006, *ApJ*, 644, 133
- Blandford R. D., McKee C. F., 1982, *ApJ*, 255, 419
- Boroson T. A., Green R. F., 1992, *ApJS*, 80, 109
- Bruzual G., Charlot S., 2003, *MNRAS*, 344, 1000
- Cid Fernandes R., Sodr e Jr. L., Vieira da Silva Jr. L., 2000, *ApJ*, 544, 123
- Cid Fernandes R. J., Aretxaga I., Terlevich R., 1996, *MNRAS*, 282, 1191
- Collier S., Peterson B. M., 2001, *ApJ*, 555, 775
- Cristiani S., Trentini S., La Franca F., Aretxaga I., Andreani P., Vio R., Gemmo A., 1996, *A&A*, 306, 395
- Cristiani S., Vio R., Andreani P., 1990, *AJ*, 100, 56
- de Vries W. H., Becker R. H., White R. L., Loomis C., 2005, *AJ*, 129, 615
- Enya K., Yoshii Y., Kobayashi Y., Minezaki T., Suganuma M., Tomita H., Peterson B. A., 2002, *ApJS*, 141, 45
- Giallongo E., Trevese D., Vagnetti F., 1991, *ApJ*, 377, 345
- Giveon U., Maoz D., Kaspi S., Netzer H., Smith P. S., 1999, *MNRAS*, 306, 637
- Helfand D. J., Stone R. P. S., Willman B., White R. L., Becker R. H., Price T., Gregg M. D., McMahon R. G., 2001, *AJ*, 121, 1872
- Hook I. M., McMahon R. G., Boyle B. J., Irwin M. J., 1994, *MNRAS*, 268, 305
- Hughes P. A., Aller H. D., Aller M. F., 1992, *ApJ*, 396, 469
- Kaspi S., Maoz D., Netzer H., Peterson B. M., Vestergaard M., Jannuzi B. T., 2005, *ApJ*, 629, 61
- Kaspi S., Smith P. S., Netzer H., Maoz D., Jannuzi B. T., Giveon U., 2000, *ApJ*, 533, 631
- Kawaguchi T., Mineshige S., Umemura M., Turner E. L., 1998, *ApJ*, 504, 671
- Kriss G., 1994, in Crabtree D. R., Hanisch R. J., Barnes J., eds, *ASP Conf. Ser. 61: Astronomical Data Analysis Software and Systems III Fitting Models to UV and Optical Spectral Data*. pp 437–+
- Krolik J. H., 1998, *Active Galactic Nuclei: From the Central Black Hole to the Galactic Environment*. Princeton University Press, 1998.
- Lacy M., Laurent-Muehleisen S. A., Ridgway S. E., Becker R. H., White R. L., 2001, *ApJ*, 551, L17
- Morgan C. W., Kochanek C. S., Morgan N. D., Falco E. E., 2006, *ApJ*, 647, 874
- Netzer H., Peterson B. M., 1997, in Maoz D., Sternberg A., Leibowitz E. M., eds, *ASSL Vol. 218: Astronomical Time Series Reverberation Mapping and the Physics of Active Galactic Nuclei*. pp 85–+
- Pereyra N. A., Vanden Berk D. E., Turnshek D. A., Hillier D. J., Wilhite B. C., Kron R. G., Schneider D. P., Brinkmann J., 2006, *ApJ*, 642, 87
- Peterson B. M., 1997, *Book Review: An Introduction to Active Galactic Nuclei*. Cambridge University Press, 1997
- Peterson B. M., et al. 2004, *ApJ*, 613, 682
- Refsdal S., Stabell R., Pelt J., Schild R., 2000, *A&A*, 360, 10
- Rengstorf A. W., et al. 2004a, *ApJ*, 606, 741
- Rengstorf A. W., et al. 2004b, *ApJ*, 617, 184
- Rengstorf A. W., Brunner R. J., Wilhite B. C., 2006, *AJ*, 131, 1923
- Schlegel D. J., Finkbeiner D. P., Davis M., 1998, *ApJ*, 500, 525
- Schneider D. P., et al. 2005, *AJ*, 130, 367
- Shang Z., et al. 2005, *ApJ*, 619, 41
- Terlevich R., Tenorio-Tagle G., Franco J., Melnick J., 1992, *MNRAS*, 255, 713
- Torricelli-Ciamponi G., Foellmi C., Courvoisier T. J.-L., Paltani S., 2000, *A&A*, 358, 57
- Tr evese D., Vagnetti F., 2002, *ApJ*, 564, 624
- Ulrich M.-H., Maraschi L., Urry C. M., 1997, *ARA&A*, 35, 445
- Vanden Berk D. E., et al. 2004, *ApJ*, 601, 692
- Vanden Berk D. E., et al. 2006, *AJ*, 131, 84
- Vestergaard M., 2002, *ApJ*, 571, 733
- Vestergaard M., Peterson B. M., 2006, *ApJ*, 641, 689
- Webb W., Malkan M., 2000, *ApJ*, 540, 652